Materials Advances

ROYAL SOCIETY OF CHEMISTRY

PAPER

View Article Online
View Journal | View Issue



Cite this: *Mater. Adv.*, 2024, 5, 7467

# Synthesis of a new photosensitizer for laser-mediated photodynamic therapy to kill cancer cells in gliomas†

Guangshu Liang,‡ Yining Yang,‡ Daofu Cheng, Yuyan Ma and Linping Yan *

Received 20th June 2024,
Accepted 24th August 2024

DOI: 10.1039/d4ma00637b

rsc.li/materials-advances

Managing glioma, a particularly aggressive form of brain cancer, poses significant challenges because of its inherent resistance and the intricate nature of the central nervous system. Photodynamic therapy (PDT), which uses photosensitizers to target and destroy cancer cells while minimizing damage to surrounding healthy tissues, has emerged as a novel and effective approach for glioma treatment. In this study, we designed and synthesized a novel photosensitizer, ITIC, for potential application in glioma therapy. By employing nanotechnology, we enhanced the water dispersibility of ITIC. ITIC nanoparticles (NPs) exhibit near-infrared absorbance and are light-activatable for generating reactive oxygen species (ROS), which allows for effective killing of cancer cells. Furthermore, the unique chemical structure of ITIC makes it easy to conjugate ITIC with targeting ligands to enable specific recognition and uptake by glioma cells in both *in vitro* and *in vivo* studies, thereby increasing the precision of glioma cell detection and engagement.



## Introduction

Gliomas are extremely invasive tumors that are primarily located in the brain. Unfortunately, they are often associated with a poor prognosis, frequent recurrence, and low five-year survival rates.[1–4] Existing treatments for gliomas, including surgery, radiotherapy, and chemotherapy, can yield less than ideal outcomes and significant side effects because of the complex nerve structure of the brain and the invasive nature of gliomas.[5–8]

To address these challenges, researchers are exploring drug delivery systems as promising approaches for clinical therapy.[9–11] One noteworthy approach, which is garnering attention, is photodynamic therapy (PDT), a noninvasive and precisely targeted cancer treatment method.[12–16] PDT involves the administration of a photosensitizer, followed by the application of light of specific wavelengths to generate reactive oxygen species (ROS),[17] which leads to the destruction of tumor cells.[18] PDT offers optimism for more effective future treatments. Photosensitizers (PSs) play a crucial role in PDT, and an ideal PS should possess high phototoxicity, low dark toxicity, and excellent stability.[19,20] Photodynamic therapy has proven to be safe and effective in treating various cancers, including intracranial malignant gliomas, resulting in significant attention from the medical community.[21–24] The success of photodynamic therapy (PDT) in treating gliomas depends on the activation of photosensitizers that accumulate in the tumor.[25–28] To address this requirement, we propose a drug delivery strategy.[14,29–31] A promising photosensitizer, designated ITIC (Scheme 1), which can improve the effectiveness of PDT for antitumor therapy, has been identified. PDT has several advantages, such as minimal systemic toxicity and noninvasiveness, over traditional therapies. The success of PDT relies on the ability of photosensitizers to generate reactive oxygen species (ROS), which can cause apoptosis of tumor cells by oxidizing cellular components such as mitochondria and nuclei.

## Experimental section

### Materials and equipment

All the necessary reagents were obtained from Sigma–Aldrich and were used without purification. The human glioblastoma U87MG cells used in this study were acquired from the Cell Bank of the Shanghai Institute of Biochemistry and Cell Biology, Chinese Academy of Sciences (CAS). For spectroscopic

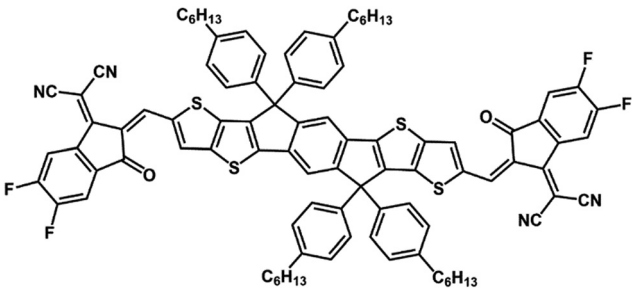


Scheme 1 The structure of ITIC.

*Department of Clinical Laboratory, Jiangsu Cancer Hospital & Jiangsu Institute of Cancer Research & The Affiliated Cancer Hospital of Nanjing Medical University, Nanjing 210009, China. E-mail: yanlinping@njmu.edu.cn*

† Electronic supplementary information (ESI) available. See DOI: https://doi.org/10.1039/d4ma00637b

‡ These authors contributed equally to this work.

analysis, $^{1}$H NMR and $^{13}$C NMR spectra were measured in $CDCl_3$ by using a Bruker DRX NMR spectrometer operating at 400 MHz, with the residual solvent used as the internal standard. UV-vis spectra were obtained by using a UV-3600 spectrophotometer from Agilent. The morphology and structure of ITIC nanoparticles were determined *via* transmission electron microscopy (TEM) and dynamic light scattering (DLS) (JEM-2100, JEOL). Cell apoptosis was analyzed *via* a flow cytometer (BD Biosciences, USA).

### Synthesis and characterization of ITIC

ITIC was prepared *via* a condensation reaction by treating ITC (0.1 mmol) and malononitrile (0.25 mmol) with ammonium acetate (0.25 mmol) and potassium carbonate (0.25 mmol) (Fig. S1, ESI†). $^{1}$H NMR 7.79 (2H, s), 7.48 (2H, s), 7.32–7.28 (2H, d, $J$ = 4.0 Hz), 7.24 (2H, s), 7.17–7.13 (2H, d, $J$ = 4.0 Hz), 7.05 (2H, s), 6.96 (2H, s), 4.09–4.03 (4H, m), 2.03–2.88 (4H, m), 2.81–2.72 (8H, m), 1.83–1.76 (2H, m), 1.74–1.64 (14H, m), 1.46–1.29 (54H, m), 0.97–0.88 (24H, m). $^{13}$C NMR: 192.02, 167.37, 141.77, 138.47, 137.09, 136.90, 135.58, 135.46, 134.77, 134.47, 130.92, 128.80, 126.20, 124.78, 122.86, 120.09, 44.83, 40.85, 31.33, 29.43, 25.95, 22.53, 14.26, 14.17, 14.01, 10.97. MALDI-TOF calculated: 1498.49, found: 1498.65.

### Calculation of the ROS quantum yield in DCM

The ROS quantum yield ($^{1}O_2$ QY) of ITIC was determined with 1,3-diphenylisobenzofuran (DPBF) as the $^{1}O_2$ indicator, with methylene blue (MB) as the standard substance. A mixture of DPBF and ITIC in DCM was prepared, with the DPBF absorbance adjusted to 1.0 and the ITIC absorbance adjusted to approximately 0.2–0.3. After the mixture was exposed to laser irradiation (660 nm), UV-vis spectra were recorded at different time intervals. The ROS quantum yield was subsequently calculated according to eqn (1).

$$\Phi_{\Delta(\mathrm{ITIC})} = \Phi_{\Delta(\mathrm{MB})} \times \frac{S_{\mathrm{PS}}}{S_{\mathrm{MB}}} \times \frac{F_{\mathrm{MB}}}{F_{\mathrm{PS}}} \quad (1)$$

where MB stands for methylene blue, $S$ is the slope of a plot of the absorbance of DPBF (at 418 nm) *versus* the irradiation time, and $F$ is calculated as $F = 1\text{–}10^{-\mathrm{OD}}$, where OD represents the optical density of the sample and MB at 660 nm.

### Preparation of ITIC NPs

To prepare ITIC NPs, a blend of ITIC (2 mg) and DSPE-$PEG_{-2000}$ (20 mg) was dissolved in tetrahydrofuran (THF). This blend was then added to 5 mL of distilled water under ultrasonication conditions. The mixture was subsequently transferred to a fume hood to extract tetrahydrofuran and was kept in a dimly lit area for later use. THF was removed through vacuum evaporation, and the ITIC NPs were filtered through a 220-nm filtration membrane for further application.

### Cell culture

To maintain U87MG cells, DMEM (Gibco, Thermo Fisher Scientific) with 10% fetal bovine serum (FBS; Gibco, Thermo Fisher Scientific) was used. The culture medium contained 100 units $mL^{-1}$ penicillin and 100 mg $mL^{-1}$ streptomycin. The cells were kept in a humidified incubator with 5% $CO_2$ at 37 °C.

### MTT assay

To determine the viability of U87MG cells, a 3-(4,5-dimethylthiazol-2-yl)-2,5-diphenyltetrazolium bromide (MTT) colorimetric assay was conducted. The cells were seeded into 96-well plates at a concentration of $1 \times 10^4$ per well in 100 μL of culture medium and incubated for 24 hours before exposure to various concentrations of ITIC NPs for specified times. The control cells were treated with 0.5% DMSO. In the illumination group, the cells were irradiated with a laser (660 nm, 0.5 W $cm^{-2}$) for 5 minutes. The cells were incubated for an additional 12 hours after irradiation. Next, 10 μL of the MTT solution (5 mg $mL^{-1}$ in PBS) was added, and the mixture was incubated for 4 hours. The supernatants were removed, and 100 μL of DMSO per well was added to dissolve the formazan crystals. The absorbance was measured at 492 nm by using a Thermo Mk3 microplate reader. A cell growth inhibition curve was generated by plotting cell growth inhibition against the drug concentration, and the half-maximal inhibitory concentration ($IC_{50}$) was determined by using the GraphPad Prism 8 software (GraphPad Software, Inc., La Jolla, CA, USA).

### Fluorescence imaging of intracellular reactive oxygen species (ROS)

A green fluorescent probe, 6-carboxy-2′,7′-dichlorofluorescein diacetate (DCF-DA; Sigma–Aldrich) was used to measure the intracellular ROS levels. U87MG cells were placed into a confocal dish and exposed to ITIC NPs (at a concentration of 10 μg $mL^{-1}$) in the medium for 24 hours. After that, the cells were stained with 2 mL of DCFH-DA (10 μM) at 37 °C for 20 minutes. The cells were washed three times with PBS and exposed to laser irradiation (660 nm, 0.5 W $cm^{-2}$) for 10 minutes. Fluorescence images were captured by using an Olympus IX 70 inverted microscope at an excitation wavelength of 633 nm, and the DCF signals were collected from 500 to 600 nm.

### Annexin V-FITC/propidium iodide (PI) staining

The analysis of apoptosis involved dual staining with annexin V-FITC and propidium iodide (PI). Following treatment with ITIC NPs, U87MG cells were collected and subsequently stained by using an annexin V-FITC/PI cell apoptosis detection kit (KeyGen Biotech, Nanjing, China). The cell apoptosis rates were then assessed *via* a flow cytometer (BD, San Jose, CA, USA), with or without prior irradiation.

### Live and dead cell assay

To assess the effect of ITIC NPs on the viability of U87MG cells, we utilized a live/dead cell double-staining kit sourced from Sigma–Aldrich Trading Co., Ltd. This kit includes calcein-AM and PI, which fluorescently stain viable and dead cells, respectively. Following the manufacturer's guidelines, we analyzed the slides with a confocal microscope.

### Antitumor effects on a nude mouse xenograft tumor model

Female BALB/c nude mice aged between 4 and 5 weeks were procured from the Comparative Medicine Center of Yangzhou

University. The study was granted approval by the Clinical Research Ethics Committee of Nanjing Medical University [ethical permit number (2023) 233]. The animal experiments followed the regulatory guidelines governing the ethical treatment of animals intended for research purposes. Nude mice were injected subcutaneously with U87MG cells at a density of $5 \times 10^6$ cells per 100 μL of serum-free medium, and tumor growth was monitored every other day. When the tumor volume reached approximately 100 $mm^3$, the mice were randomly distributed into the following three groups: (i) the control group; (ii) the no illumination group; and (iii) the illumination group. The mice in both the illumination and no illumination groups were injected ITIC NPs at a dose of 10 μg (100 μg $mL^{-1}$, 100 μL) *via* the tail vein, while the control group was administered PBS. After administration, the tumors in the control and illumination groups were irradiated with a 660 nm laser for 8 minutes. The no illumination group did not receive any irradiation. The tumor volume ($V$) was measured daily to observe dynamic changes in tumor growth and was calculated according to the following formula: $V\,(mm^3)$ = length × width$^2$ × 0.5. The treatment process spanned twenty days, during which the tumor volume and body weight of the mice were monitored every two days. After the treatment ended, all the nude mice were euthanized, and the tumor tissues were extracted and subjected to histopathological analysis. Additionally, major organs, such as the heart, liver, spleen, lung, and kidney, were also extracted and evaluated for evidence of drug toxicity.

## Results and discussion

### Synthesis and characterization of ITIC and NPs

ITIC was synthesized through a condensation reaction and characterized by $^1$H NMR, $^{13}$C NMR, and MALDI-TOF (Fig. S2–S4, ESI†), with the results confirming its purity. In cancer nanomedicine, nanoformulations significantly improve colloidal stability and stealth effects. DSPE-PEG$_{-2000}$ was used to encapsulate ITIC to prepare water-dispersible nanoparticles. DLS analysis revealed that the ITIC NPs exhibited excellent dispersion and had an average diameter of 54 nm (Fig. 1a), which was consistent with the TEM results (Fig. 1b). The ITIC NPs were also stable under physiological conditions, with their diameter remaining similar in DMEM and PBS (Fig. S5, ESI†). To illustrate their light-responsive characteristics, absorbance and fluorescence spectra were recorded. As depicted in Fig. 1c, ITIC displays a broad absorbance spectrum, spanning from 550 to 750 nm, with a peak at 676 nm, whereas a notable redshift is evident for the nanoparticles, with a peak at 739 nm. This shift was similarly observed in the emission spectra (Fig. 1d).

### ROS generation, MTT assay, and flow cytometry results

The capacity to generate reactive oxygen species (ROS) serves as a gauge of the potential of a photosensitizer for inducing significant phototoxicity. To assess the ROS generation capability of ITIC nanoparticles in response to light exposure, we employed a marker known as DPBF, as illustrated in Fig. 2a and b. The effective

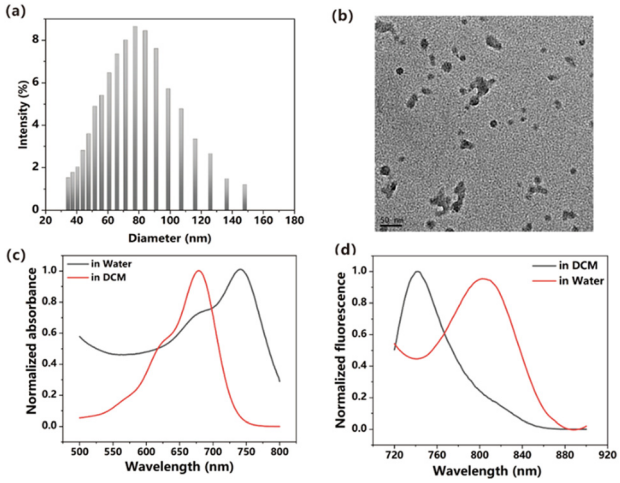


Fig. 1 (a) DLS of ITIC NPs in water. (b) TEM image of ITIC NPs. (c) Absorbance spectra of ITIC NPs in DCM and NPs in water. (d) Emission spectra of ITIC in DCM and NPs in water.

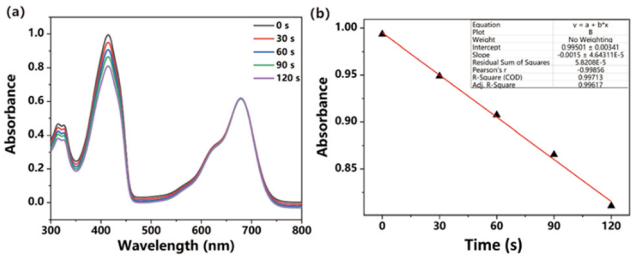


Fig. 2 (a) Absorbance of DPBF degraded upon irradiation. (b) Linear fitting of time *versus* absorbance.

generation of ROS was inferred from the degradation of DPBF observed at 414 nm, which was attributed to its oxidation, ultimately resulting in its decomposition. The calculated ROS quantum yield was 10.27% when methylene blue (MB) was used as a standard substance. (Fig. S6, ESI†). The ROS generation ability is lower than that of DPPA,[32] DPPTPE[33] but higher than that of BDPTPA and BDPA.[34]

An *in vitro* investigation was carried out by employing U87MG cells to demonstrate the enhanced photodynamic therapeutic efficacy of ITIC nanoparticles (NPs). The cellular uptake of the ITIC NPs was examined *via* a confocal live cell imaging system. As depicted in Fig. 3, the results revealed that the ITIC nanoparticles were efficiently internalized by the cells (red channel) and exhibited substantial generation of reactive oxygen species (ROS) upon light exposure (green channel). The nonfluorescent

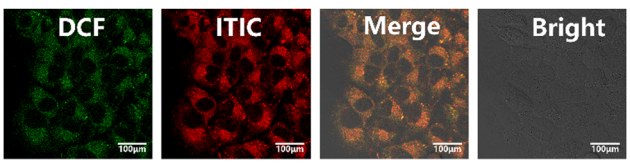


Fig. 3 Cellular uptake of and ROS generation by ITIC NPs in irradiated U87MG cells.

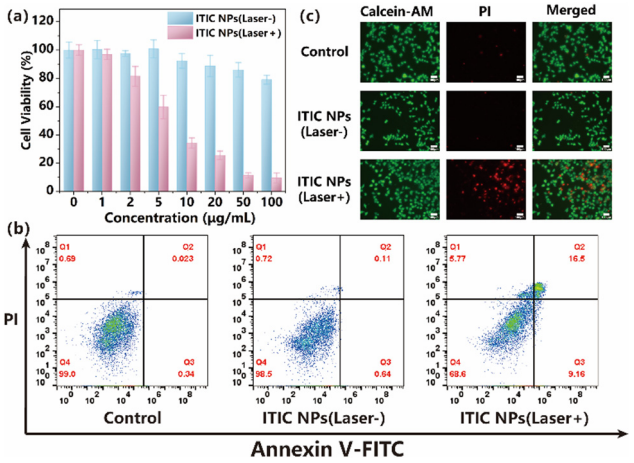


Fig. 4 (a) MTT assay results for U87MG cells treated with ITIC NPs with/without irradiation. (b) Flow cytometry results for U87MG cells in the control, ITIC NPs only, and ITIC NPs + laser groups. (c) Live and dead cells costained with calcein-AM/PI.

DCF-DA underwent a transformation into fluorescent DCF in the presence of ROS, and all signals seamlessly merged.

The inhibitory potential of various concentrations of ITIC NPs on the growth of U87MG cells was evaluated. Following a 24-hour incubation of the cells with ITIC NPs, an MTT assay was conducted and yielded an $IC_{50}$ value of 7.08 μg $mL^{-1}$ with laser irradiation, as illustrated in Fig. 4a. Importantly, the incubation of the cells with the NPs in the absence of light exposure resulted in minimal toxicity. The phototoxicity of ITIC NPs was lower than that of the previously reported DPPTPA (4.38 mg $mL^{-1}$)[35] but higher than that of PDPP (13.84 mg $mL^{-1}$).[36]

An annexin V-FITC/PI double-staining assay was subsequently employed to confirm the proapoptotic effects of the ITIC NPs. Compared with the control group, the U87MG cells in the illuminated group showed significantly elevated apoptotic rates following treatment with ITIC NPs (Fig. 4b). These findings demonstrated that ITIC NPs induced typical apoptosis in U87MG cells, with minimal dark toxicity in the absence of illumination.

Moreover, to further assess the therapeutic efficacy of ITIC NPs *in vitro*, calcein-AM/PI costaining was used (Fig. 4c). Neither the control group nor the ITIC NP (laser−) group exhibited noticeable red fluorescence. However, following laser irradiation, the ITIC NP (laser+) group presented the highest incidence of cell death, indicating an exceptional synergistic antitumor effect. These findings aligned with those obtained by flow cytometry analysis. In summary, ITIC NPs effectively achieved the anticipated synergistic phototherapeutic effect.

### *In vivo* phototherapy

The present study aimed to investigate the efficacy of *in vivo* photodynamic therapy (PDT) in treating glioma tumors with ITIC NPs. Nude mice with glioma tumors were used for this purpose. The findings of the present study indicated that the relative tumor volumes in the control and no illumination groups increased almost 10-fold. However, the relative tumor volume in the group treated with ITIC NPs with laser irradiation increased only 1.2-fold by the end of the study. These observations suggest that ITIC NPs exhibit significant phototoxicity and efficacy in treating tumors. Representative tumor images in the three groups are shown in Fig. 5b. To evaluate the potential toxicity of ITIC NPs, weight changes in the nude mice were monitored. The results revealed that there were no significant differences in the weights of the nude mice among the groups. These findings indicate that ITIC NPs have low dark toxicity. After treatment, the tumors and normal organs, including the heart, liver, spleen, lung, and kidneys, were collected. Hematoxylin and eosin (H&E)-stained images of the tumors revealed that the nuclei were damaged in the ITIC NP (laser+) group. In contrast, those in the control and ITIC NP (laser−) groups were in good condition. The TUNEL results further indicated that the number of positive cells in the tumor tissues from the ITIC NP (laser+) treatment group was significantly greater than those in the control and ITIC NP (laser−) groups. The H&E-stained images of normal organs are presented in Fig. 5e. Compared with that in the control group, no discernible tissue damage was observed in the ITIC NP treatment groups. The study concluded that under irradiation, ITIC NPs could exhibit antitumor activity, and the results suggest minimal toxicity of ITIC NPs *in vivo* and significant potential for clinical application.

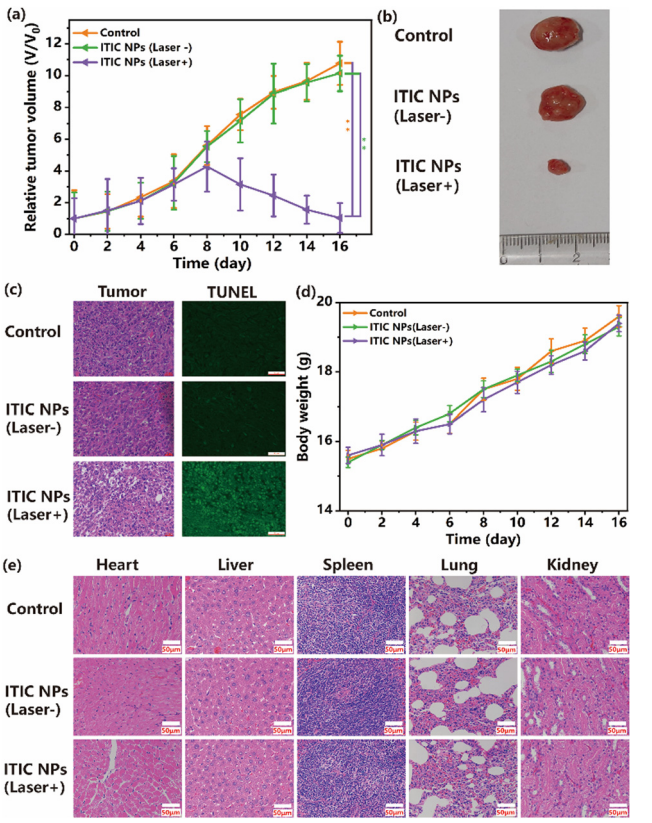


Fig. 5 (a) Tumor volume changes in the mice (**$P < 0.01$). (b) Representative images of tumors. (c) H&E and TUNEL staining images of the tumors in the control, ITIC NP (laser−) and ITIC NP (laser+) groups. (d) Body weight changes. (e) H&E images of the heart, liver, spleen, lung, and kidney.

## Conclusion

In conclusion, our research led to the development of a novel photosensitizer, termed ITIC, which exhibited an exceptional capability for generating reactive oxygen species (ROS). The ITIC nanoparticles had a diameter of less than 100 nm and exhibited good dispersity in water. Upon exposure to laser light, these nanoparticles effectively penetrated cells and generated ROS, resulting in potent phototoxicity that led to the elimination of U87MG cells. Furthermore, these nanoparticles exhibited minimal toxicity in the absence of laser light, indicating their favorable biocompatibility. Moreover, an *in vivo* investigation demonstrated that ITIC nanoparticles could suppress tumor proliferation with the assistance of laser irradiation, which provides evidence that ITIC nanoparticles can be used in preclinical trials. These findings underscore the potential utility of ITIC nanoparticles as a promising new option for cancer treatment.

## Author contributions

Guangshu Liang was mainly responsible for the synthesis and characterization of compounds. Yining Yang was mainly responsible for the cell experiments and data collection. Daofu Cheng was responsible for the data analysis and writing of the manuscript. Guangshu Liang and Yuyan Ma were responsible for the animal experiments and drug administration *in vivo*. Linping Yan was mainly responsible for the experimental design and guidance.

## Data availability

No primary research results, software or code have been included and no new data were generated or analysed as part of this review.

## Conflicts of interest

The authors do not have any conflicts of interest to declare.

## Acknowledgements

The authors acknowledge the financial support from the Research Fund of the Jiangsu Cancer Hospital (grant number: ZM202019) and the Medical Research Program of the Jiangsu Health Commission (grant number: M2022106).

## Notes and references

1 E. S. Pierce, Baseballs, tennis balls, livestock farm manure, the IDH1 mutation, endothelial cell proliferation and hypoxic pseudopalisading (granulomatous) necrosis: Mycobacterium avium subspecies paratuberculosis and the epidemiology, cellular metabolism and histology of diffuse gliomas, including glioblastoma, *Open Vet. J.*, 2019, **9**, 5–12.

2 Q. T. Ostrom, H. Gittleman, L. Stetson, S. Virk and J. S. Barnholtz-Sloan, Epidemiology of Intracranial Gliomas, *Prog. Neurol. Surg.*, 2018, **30**, 1–11.

3 M. E. Davis, Epidemiology and Overview of Gliomas, *Semin. Oncol. Nurs.*, 2018, **34**, 420–429.

4 A. Perry and P. Wesseling, Histologic classification of gliomas, *Handb. Clin. Neurol.*, 2016, **134**, 71–95.

5 Q. T. Ostrom, H. Gittleman, L. Stetson, S. M. Virk and J. S. Barnholtz-Sloan, Epidemiology of gliomas, *Cancer Treat. Res.*, 2015, **163**, 1–14.

6 I. Qaddoumi, I. Sultan and A. Gajjar, Outcome and prognostic features in pediatric gliomas: a review of 6212 cases from the Surveillance, Epidemiology, and End Results database, *Cancer*, 2009, **115**, 5761–5770.

7 D. M. Lemke, Epidemiology, diagnosis, and treatment of patients with metastatic cancer and high-grade gliomas of the central nervous system, *J. Infus. Nurs.*, 2004, **27**, 263–269.

8 N. Patil, M. E. Kelly, D. N. Yeboa, R. A. Buerki, G. Cioffi, S. Balaji, Q. T. Ostrom, C. Kruchko and J. S. Barnholtz-Sloan, Epidemiology of brainstem high-grade gliomas in children and adolescents in the United States, 2000-2017, *Neuro-Oncol.*, 2021, **23**, 990–998.

9 J. Zhou, J. Zhang, Y. Sun, F. Luo, M. Guan, H. Ma, X. Dong and J. Feng, A nano-delivery system based on preventing degradation and promoting absorption to improve the oral bioavailability of insulin, *Int. J. Biol. Macromol.*, 2023, **244**, 125263.

10 Z. Chen, Y. Liu, Y. Yu, S. Yang, J. Feng, Y. Zhu, W. Huang, B. Qin, X. Guan, Z. He, M. Sun and J. Sun, Micro-to-nano Oncolytic Microbial System Shifts from Tumor Killing to Tumor Draining Lymph Nodes Remolding for Enhanced Immunotherapy, *Adv. Mater.*, 2023, e2306488, DOI: **10.1002/adma.202306488**.

11 K. Kopeckova, T. Eckschlager, J. Sirc, R. Hobzova, J. Plch, J. Hrabeta and J. Michalek, Nanodrugs used in cancer therapy, *Biomed. Pap. Med. Fac. Univ. Palacky Olomouc Czech Repub.*, 2019, **163**, 122–131.

12 A. Amirjani, P. Shokrani, S. A. Sharif, H. Moheb, H. Ahmadi, Z. S. Ahmadiani and M. S. Paroushi, Plasmon-enhanced nano-photosensitizers: game-changers in photodynamic therapy of cancers, *J. Mater. Chem. B*, 2023, **11**, 3537–3566.

13 B. Ji, M. Wei and B. Yang, Recent advances in nanomedicines for photodynamic therapy (PDT)-driven cancer immunotherapy, *Theranostics*, 2022, **12**, 434–458.

14 A. Warrier, N. Mazumder, S. Prabhu, K. Satyamoorthy and T. S. Murali, Photodynamic therapy to control microbial biofilms, *Photodiagn. Photodyn. Ther.*, 2021, **33**, 102090.

15 L. Lin, X. Song, X. Dong and B. Li, Nano-photosensitizers for enhanced photodynamic therapy, *Photodiagn. Photodyn. Ther.*, 2021, **36**, 102597.

16 E. J. Prazmo, M. Kwasny, M. Lapinski and A. Mielczarek, Photodynamic Therapy As a Promising Method Used in the Treatment of Oral Diseases, *Adv. Clin. Exp. Med.*, 2016, **25**, 799–807.

17 S. Kwiatkowski, B. Knap, D. Przystupski, J. Saczko, E. Kedzierska, K. Knap-Czop, J. Kotlinska, O. Michel, K. Kotowski and

J. Kulbacka, Photodynamic therapy-mechanisms, photosensitizers and combinations, *Biomed. Pharmacother.*, 2018, **106**, 1098–1107.

18 B. Niu, K. Liao, Y. Zhou, T. Wen, G. Quan, X. Pan and C. Wu, Application of glutathione depletion in cancer therapy: Enhanced ROS-based therapy, ferroptosis, and chemotherapy, *Biomaterials*, 2021, **277**, 121110.

19 K. Wang, B. Yu and J. L. Pathak, An update in clinical utilization of photodynamic therapy for lung cancer, *J. Cancer*, 2021, **12**, 1154–1160.

20 M. Penetra, L. G. Arnaut and L. C. Gomes-da-Silva, Trial watch: an update of clinical advances in photodynamic therapy and its immunoadjuvant properties for cancer treatment, *Oncoimmunology*, 2023, **12**, 2226535.

21 S. Kaneko, S. Fujimoto, H. Yamaguchi, T. Yamauchi, T. Yoshimoto and K. Tokuda, Photodynamic Therapy of Malignant Gliomas, *Prog. Neurol. Surg.*, 2018, **32**, 1–13.

22 K. Mahmoudi, K. L. Garvey, A. Bouras, G. Cramer, H. Stepp, J. G. Jesu Raj, D. Bozec, T. M. Busch and C. G. Hadjipanayis, 5-aminolevulinic acid photodynamic therapy for the treatment of high-grade gliomas, *J. Neurooncol.*, 2019, **141**, 595–607.

23 T. Hsia, J. L. Small, A. Yekula, S. M. Batool, A. K. Escobedo, E. Ekanayake, D. G. You, H. Lee, B. S. Carter and L. Balaj, Systematic Review of Photodynamic Therapy in Gliomas, *Cancers*, 2023, **15**, 3918.

24 X. Dong, Y. Zeng, Z. Zhang, J. Fu, L. You, Y. He, Y. Hao, Z. Gu, Z. Yu, C. Qu, X. Yin, J. Ni and L. J. Cruz, Hypericin-mediated photodynamic therapy for the treatment of cancer: a review, *J. Pharm. Pharmacol.*, 2021, **73**, 425–436.

25 H. Z. Xu, T. F. Li, Y. Ma, K. Li, Q. Zhang, Y. H. Xu, Y. C. Zhang, L. Zhao and X. Chen, Targeted photodynamic therapy of glioblastoma mediated by platelets with photocontrolled release property, *Biomaterials*, 2022, **290**, 121833.

26 X. Lin, F. Chen, X. Yu, H. Wang, H. Qiu, Y. Li, S. Yin and P. J. Stang, Phenylthiol-BODIPY-based supramolecular metallacycles for synergistic tumor chemo-photodynamic therapy, *Proc. Natl. Acad. Sci. U. S. A.*, 2022, **119**, e2203994119.

27 Z. Lv, L. Jin, W. Gao, Y. Cao, H. Zhang, D. Xue, N. Yin, T. Zhang, Y. Wang and H. Zhang, Novel YOF-Based Theranostic Agents with a Cascade Effect for NIR-II Fluorescence Imaging and Synergistic Starvation/Photodynamic Therapy of Orthotopic Gliomas, *ACS Appl. Mater. Interfaces*, 2022, **14**, 30523–30532.

28 M. Norouzi, Gold Nanoparticles in Glioma Theranostics, *Pharmacol. Res.*, 2020, **156**, 104753.

29 V. Sunil, J. H. Teoh, B. C. Mohan, A. Mozhi and C. H. Wang, Bioengineered immunomodulatory organelle targeted nanozymes for photodynamic immunometabolic therapy, *J. Controlled Release*, 2022, **350**, 215–227.

30 S. Wang, G. Yu, W. Yang, Z. Wang, O. Jacobson, R. Tian, H. Deng, L. Lin and X. Chen, Photodynamic-Chemodynamic Cascade Reactions for Efficient Drug Delivery and Enhanced Combination Therapy, *Adv. Sci.*, 2021, **8**, 2002927.

31 X. Li, X. Geng, Z. Chen and Z. Yuan, Recent advances in glioma microenvironment-response nanoplatforms for phototherapy and sonotherapy, *Pharmacol. Res.*, 2022, **179**, 106218.

32 J. Shen, L. Pan, X. Zhang, Z. Zou, B. Wei, Y. Chen, X. Tang and D. Zou, Delivering singlet oxygen in dark condition with an anthracene functionalized semiconducting compound for enhanced phototheranostics, *Front. Bioeng. Biotech.*, 2022, **10**, 781766.

33 J. Zou, J. Zhu, Z. Yang, L. Li, W. Fan, L. He, W. Tang, L. Deng, J. Mu, Y. Ma, Y. Cheng, W. Huang, X. Dong and X. Chen, A Phototheranostic Strategy to Continuously Deliver Singlet Oxygen in the Dark and Hypoxic Tumor Microenvironment, *Angew. Chem., Int. Ed.*, 2020, **59**, 8833–8838.

34 J. Zou, L. Li, J. Zhu, X. Li, Z. Yang, W. Huang and X. Chen, Singlet oxygen ''afterglow'' therapy with NIR-II fluorescenct molecules, *Adv. Mater.*, 2021, **33**, 2103627.

35 C. Yin, X. Bao, J. Li, J. Zhu and J. Sui, A triphenylamine functionalized photosensitizer as a promising candidate for osteosarcoma cancer phototheranostics, *Mater. Adv.*, 2024, **5**, 5134.

36 J. Zhu, Y. Zhang, Z. Li, X. Bao, Y. Zhou, B. Ma, Y. Xie, P. Yan, Z. Wu, Q. Zhang, J. Zou and X. Chen, Tumor-microenvironment-responsive poly-prodrug encapsulated semiconducting polymer nanosystem for phototherapy-boosted Chemotherapy, *Mater. Horiz.*, 2023, **10**, 3014–3023.